# Experimental report

10/09/2024

**Proposal:** EASY-1182 **Council:** 4/2023

**Title:** Exploring the Relationship Between Halide Substitution, Structural disorder, and Li+ Distribution in Lithium Argyrodites Li6-xAsS5-xBr1+x

**Research area:** Materials

**This proposal is a new proposal**


**Main proposer:** Ajay GAUTAM

**Experimental team:**

**Local contacts:** Emmanuelle SUARD


**Samples:** Li6-xAsS5-xBr1+x x=0

| Instrument | Requested days | Allocated days | From | To |
|---|---|---|---|---|
| D2B | 8 | 8 | 14/09/2023 | 15/09/2023 |


## Abstract:

Lithium argyrodite superionic conductors have recently gained significant attention as potential solid electrolytes for all-solid-state batteries because of their high ionic conductivity and ease of processing. Promising aspects of these materials are the ability to introduce different halide (Li6-xAsS5-xHal1+x, Hal = Cl and Br) into the crystal structure, which can greatly impact the lithium distribution over the wide range of accessible sites and the structural site disorder which both strongly influence the ionic conductivity. However, the relationship between halide substitution, structural site disorder, and lithium distribution is not fully understood. In this study, we investigate the Bromide substitution on lithium argyrodite Li6-xAsS5-xBr1+x and identified the solubility limit by changing the synthesis protocol. Here we plan neutron diffraction experiments on Br- substituted Li6-xAsS5-xBr1+x solid solutions, which will shed light on the Li-distribution and elucidate the structure-property relationships in this system.

Lithium argyrodite thiophosphate superionic conductors are being explored as promising solid electrolytes for all-solid-state batteries, primarily due to their high ionic conductivity and ease of processing. Yet, these electrolytes present challenges such as chemical instability in humid conditions and incompatibility with cathode materials. Although some lithium argyrodites show improved air stability, their ionic conductivity deteriorates below the practically required value. Here we explore new compositions of lithium argyrodite, $Li_{6-x}AsS_{5-x}Br_{1+x}$ (for $0.0 \leq x \leq 0.6$), which could improve air stability and higher ionic conductivity. However, the underlying changes to the lithium substructure-ionic transport were not investigated. Along with the negative x-ray scattering factor of lithium another problem to study these materials via XRD. Thus, to shed light into the lithium-ion conduction mechanism, here we explore neutron diffraction studies for a large range of nominal halide compositions in this material to understand the lithium substructure and correlated ionic transport. (Manuscripts under preparation)

The $Li_{6-x}AsS_{5-x}Br_{1+x}$ series are synthesized via facile solid-state reaction. The final hand-ground composition were used neutron diffraction studies. The room temperature neutron powder diffraction data were collected on the D2B high-resolution powder diffractometer at the Institute Laue-Langevin beamline (ILL, Grenoble, France), with monochromatic neutron wavelength $\lambda$ = 1.594 Å, and each data collection required 4 hours.

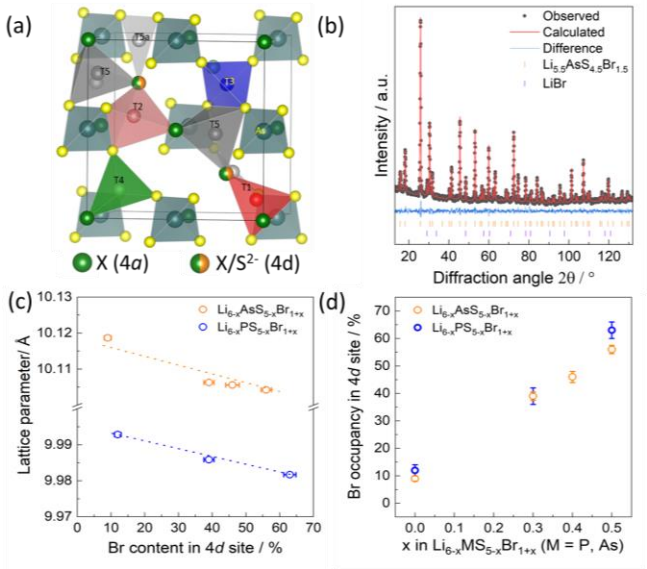


***Figure 1.*** *(a) $Li_{6-x}AsS_{5-x}X_{1+x}$ argyrodite framework. (b) Analysis of neutron diffraction data via Rietveld refinement of $Li_{5.5}AsS_{4.5}Br_{1.5}$. (c) Lattice parameter with Br occupancy at the Wyckoff 4d position. (d) Bromide occupancy in Wyckoff 4d position as a function of total bromide content.*

Figure 1a shows the lithium argyrodite structure, where $X^-$ and $S^{2-}$ at the 4d site, with $X^-$ occupying the 4a site. The lithium argyrodite framework has 136 interstitial voids, 4 voids are occupied by $(As/P)^{5+}$, forming $(As/P)S_4^{3-}$ units. The remaining voids can be occupied by lithium with different configurations: T1 (red), T2 (pink), T3 (blue), T4 (green), and T5 (grey). Figure 1b

shows a Rietveld refinement of one composition of this series *i.e.* $Li_{5.5}AsS_{4.5}Br_{1.5}$ Rietveld refinement of Neutron diffraction data observed the $Li_{6-x}AsS_{5-x}Br_{1+x}$ series exhibited a cubic structure across all compositions, assigned to the $F\bar{4}3m$ space group, the solubility limit was found at x = 0.5, indicating that free $S^{2-}$ is not entirely substitutable by the bromide anion. We observe the pronounced emergence of LiBr (8 wt%) and $Li_3AsS_4$ (2.2 wt%) side-phases at compositions of x = 0.6 as seen in the neutron diffraction data. This suggests the solubility limit for this series lies between 0.5 and 0.6. The remaining samples contained minor impurity phases of LiBr (up to 3.0 wt%), but these impurities were unlikely to impact ionic transport or structural analysis. With an increase in Br content in the thioarsenate series, the lattice parameters correspondingly decrease, although the Br occupancy at the 4*a* site remains relatively unchanged which is associated with the unit cell parameter. This observation aligns with previous findings ($Li_{6-x}PS_{5-x}Cl_{1+x}$ and $Li_{6-x}PS_{5-x}Br_{1+x}$ series ) and indicates that increased Br content induces $Li^+$ vacancies and changes in the $Li^+$ substructure, thus reducing lattice parameters. Figure 1d displays the percentage of Br at the Wyckoff 4*d* site as a function of total Br content. As the Br content (x) increases, Br is distributed across the 4*d* sites also increases within the argyrodite structure.

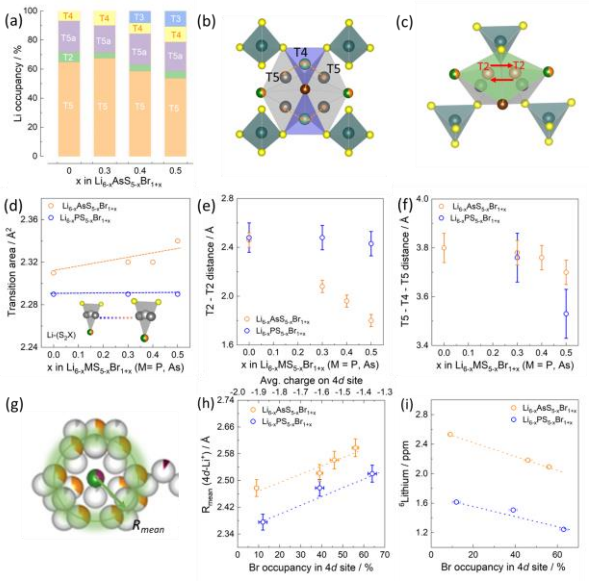


***Figure 2.*** *(a) The $Li^+$ distribution across the different sites of $Li_{6-x}AsS_{5-x}Br_{1+x}$ as a function of Br content. (b) A lithium jump pathway connecting two T5 sites via a T4 site (T5−T4−T5). (c) Second lithium jump pathway through two neighboring T2 sites (T2−T2). (d) The transition area of Li-($S_2X$) as a function of bromide content. The inter-cage lithium-ion pathway distances: (e) between T2−T2 and (f) the linked pathway from T5 through T4 to T5 as a function of bromide content. (g) The visual representation of $R_{mean}$. (h) the average $Li^+$ distribution, $R_{mean}$, representing the radius of the sphere formed by Li positions centered around the anion position (Wyckoff 4d, $S^{2-}$). As the Br content increases or the Br occupancy on 4d site increases, the average charge on the 4d site decreases as the divalent S is replaced by monovalent Br. This*

*causes $R_{mean}$ to increase, representing an expansion of lithium cage and decrease the inter-cage jump distance.(i) $^6Li$ chemical shift value of $Li_{6-x}AsS_{5-x}Br_{1+x}$ as a function of the Br content.*

Recent studies investigating the lithium substructure of $(Li_{7-x-y}(PS_4)(S_{2-x-y}Cl_xBr_y)$, and $Li_{6-x}PS_{5-x}Br_{1+x}$ found two inter-cage pathways (the first via adjacent T2 sites and the second via T5 sites through the T4 site as shown in Figures 2b and c) that appear crucial for long-range $Li^+$ diffusion. Additionally, bond valence sum calculations suggest that the inter-cage jump via the T4 site has lower energy barriers for these compositions. In the present thioarsenate series, we determined the T4 and T2 occupancies and the jump distances, T2−T2 and T5−T4−T5, as functions of bromide content, shown in Figures 2e and f. As the bromide content increases, the T2−T2 and T5−T4−T5 distances decrease. This suggests that an increase in bromide content results in shorter inter-cage distances and therefor more diffusion between the cages.

To explore how bromide affects $Li^+$ arrangement, we extended the calculation of the average $Li^+$ distribution, as expressed as the mean radius of the Li cage, $R_{mean}$, to include all sites determined by Rietveld refinement. $R_{mean}$ is calculated by averaging the distances from the central 4*d* anion (usually $S^{2-}$) to various $Li^+$ sites, and then dividing this by the number of $Li^+$ ions at specific sites within a single cage. A graphical depiction of $R_{mean}$ is presented in Figure 2g. As we increased the bromide content in the thioarsenate argyrodite, we observed a concomitant increase in the $R_{mean}$ values (see Figure 2h). A larger $R_{mean}$ value signifies an expansion of the $Li^+$ cage, which in turn shortens the T5−T4 distances, enhancing the connectivity between cages and thereby enhancing long range ionic diffusion. This observation is also corroborated by changes in chemical shift observed upon bromine addition from the room-temperature $^6Li$ MAS NMR spectra (Figure 2i). For $Li_6AsS_5Br$ the $^6Li$ resonance is observed at 2.53 ppm. As the bromide content increases, the $^6Li$ resonance shifts upfield to lower ppm values (Figure 2i) indicating that the Li-ions are more shielded. This can be explained by the positive charge lithium ion strongly attracted to S ion than Br ion at the 4*d* site in the center of the cage. This leads to an increase in $R_{mean}$ and contributes to the shift of the $^6Li$ peak to lower ppm values.

To examine the influence of Br content on the ionic conductivity of the $Li_{6-x}AsS_{5-x}Br_{1+x}$ series, we carried out temperature-dependent impedance spectroscopy to measure the ionic conductivity, With increasing the Br content, the ionic conductivity shows a dramatic increase from 2 mS/cm to 15.4 mS/cm, which to the best of our knowledge is the highest ionic conductivity obtained in the lithium argyrodites series prepared by cold pressing. Additionally, Figure 3b illustrates the diffusion coefficient obtained from with pulsed field gradient (PFG) NMR measurements, demonstrating an increase from $2.25\times10^{-12}$ to $1.6\times10^{-11}$ $m^2/s$ with the increase of bromide content. This suggests that the higher lithium diffusion coefficient is responsible for the enhancement in ionic conductivity by a factor of 7 in $Li_{5.5}AsS_{4.5}Br_{1.5}$, compared to $Li_6AsS_5Br$. This study suggests that altering the halide content in thioarsenate can modify lithium distribution, leading to improved air stability and higher ionic conductivity. Overall understanding of structure–transport correlations in argyrodites, particularly how changes in anionic charge distribution affect the $Li^+$ ion substructure.